

**Nano-confined Electrochemical Reaction Studied by
Electrochemical Surface Forces Apparatus**

Journal:	<i>Faraday Discussions</i>
Manuscript ID	FD-ART-08-2021-000060.R1
Article Type:	Paper
Date Submitted by the Author:	19-Sep-2021
Complete List of Authors:	Kasuya, Motohiro; Tohoku University, Institute of Multidisciplinary Research for Advanced Materials (IMRAM) Kubota, Daiki; Tohoku University, Institute of Multidisciplinary Research for Advanced Materials Fujii, Sho; National Institute of Technology Kisarazu College Kurihara, Kazue; Tohoku University, Institute of Multidisciplinary Research for Advanced Materials (IMRAM)

Nano-confined Electrochemical Reaction Studied by Electrochemical Surface Forces Apparatus

*Motohiro Kasuya¹, Daiki Kubota¹, Sho Fujii², Kazue Kurihara^{*1,2,3}*

¹Institute of Multidisciplinary Research for Advanced Materials, Tohoku University, Sendai 980-8577, Japan.

²Advanced Institute for Materials Research (AIMR), Tohoku University, Sendai 980-8577, Japan.

³New Industry Creation Hatchery Center, Tohoku University, Sendai 980-8578, Japan.

*E-mail: kazue.kurihara.b7@tohoku.ac.jp

Abstract

Electrochemical reactions in a nano-space are different from those in bulk solutions due to structuring of the liquid molecules and peculiar ion behavior at the electric double layer and are important for

applications involving sensors and energy devices. The electrochemical surface forces apparatus (EC-SFA) we developed enabled us to study the electrochemical reactions in a solution nano-confined between the electrodes with varying the distance (D) of nm resolution. We performed the measurements of the current-distance profiles due to electrochemical reaction of the redox couples in the electrolyte nano-confined between Pt electrodes using our EC-SFA. We observed a long-range feedback current due to redox cycling and the sudden current increase at a short distance, the latter for the first time. This sudden current increase was two orders greater than the conventional feedback current and was observed at $D < 5$ nm when approaching between the electrodes and $D < 200$ nm in separation. We simultaneously measured the electric double layer force and the current between the electrodes in the solution to study the mechanisms of this sudden current increase in the short distance range. The results revealed the molecular insight as how the redox species affect the current between two electrodes under nano-confinement. This study demonstrated that EC-SFA is a powerful tool for obtaining fundamental knowledge about the nano-confined electrochemical reactions for nanoelectrodes which can be applied to sensors and energy devices.

1. Introduction

Electrolyte solutions confined in nano-spaces exhibit different properties from those of bulk solutions due to structuring of the liquid and restricted molecular motions. For example, when ionic liquids are under confinement, they form layered structures¹ and their viscosities increase.² These viscosity increases were applied to the gelation of the electrolyte for the quasi-solid battery.³ Another example is the pH under confinement. When water is confined between negative surfaces, the pH increases. We reported that such interfacial pH changes are due to both concentrating of the proton in the electric double layer and hydration of the solid surfaces and absorbed ions.⁴

For nano-electrochemical devices, such as sensors and energy devices, their peculiar properties, fast time responses, small capacitive background, and enhanced voltametric responses are known in practice and considered as advantages.⁵⁻⁷ Therefore, various electrode configurations in small-spaces, such as the ring-disk electrode,⁸ interdigitated array electrode,⁹⁻¹⁰ ultrathin layer cell¹¹ and confined bipolar electrode,¹²⁻¹³ were developed and applied to those electrochemical devices for achieving a highly sensitive detection in simultaneous multi-sample analyses for small sample volumes. However, the mechanisms of these advantageous properties have not been well elucidated. Electrochemical reaction behaviors in nano-structured electrodes were characterized by only limited techniques such as model analysis and spatially resolved characterization methods of scanning electrochemical microscopy (SECM)

and electrochemical atomic force microscopy.¹⁴⁻¹⁷ They have been used to monitor the 2D images of the electrochemical reactions and/or electrodes with a nanometer resolution, however, there is a limitation of the low vertical spatial resolution, i.e., several tens nm, between electrodes because typical confinement effects appear at separation distances below ca. 20 nm. Therefore, a suitable characterization method for studying the confinement effects on electrochemical reactions is desired.

Another potentially powerful technique can be the surface forces measurement. This technique provides a unique tool for studying confined liquids of varying thicknesses (surface separation, D) at a 0.1 nm resolution.¹⁸⁻²⁴ By employing a surface force apparatus (SFA), we have developed novel techniques, such as the resonance shear measurement (RSM),²³⁻²⁵ X-ray diffraction apparatus,²⁶ and SFA fluorescence spectroscopy^{4,27}, and studied the behavior of confined liquids.

Electrochemical (EC)-SFA has been another direction for the development of SFA. The EC-SFA can directly monitor the electric double layer forces as a function of the surface separation and quantitatively estimate the surface potential and charges of the electrodes.²⁸⁻³⁰ Naturally, there were interests in developing EC-SFA. Conner and Horn succeeded in measuring the interactions between mica and a mercury droplet which was connected to a potentiostat.²⁹ Vanderlick measured the interactions between mica and a gold electrode.³⁰ However, these EC-SFAs used the conventional SFA with FECO

(fringes of equal chromatic order) for the distance determination, and at least one transparent substrate (typically mica) was required.^{29,30} This condition renders the analysis of interactions more difficult due to asymmetric configurations, and it is impossible to study two electrodes under various applied potentials. We recently developed a new-type of surface forces apparatus, i.e., the twin-path SFA, using the modified two-beam (twin-path) interferometry for measuring the interactions between nontransparent substrates.³¹ Based on this twin-path SFA, we developed a new type of EC-SFA which enables us to measure the interaction between non-transparent electrodes in a symmetric configuration.²⁸ We applied this EC-SFA (twin-path type) for characterizing non-transparent electrodes such as gold and platinum.³²⁻³⁴ These studies revealed how the surface potentials and charge density were affected by the various selectively adsorbed anions on the gold electrode and the hydrogen adsorption on the platinum electrodes.³²⁻³³ We also studied charge neutralization of the ferrocene modified electrode by counterions and quantitatively evaluated the effective charges on the electrode and the ratio of the strongly bound counterions and the loosely bound counterions in the Stern layer.³⁴

Taking advantage of the precise control of the separation distance of SFA, Fan and Bard studied the currents between two very thin Pt electrodes deposited on mica by changing the separation. However, their instrument could not determine the distance shorter than 500 nm, therefore, assumed the zero distance

from the point which showed the sudden current increase and estimated the distance from the approaching speed of the electrodes. They also did not measure the forces between the electrodes. The EC-SFA we developed enabled us to study both the force and the current between the electrodes by varying their distances with a nm resolution. The measured force profiles provided important information, such as surface potentials, charge densities and ion adsorption of the electrodes, which could be useful for understanding the detailed mechanisms of the observed electrochemical events under nano-confinement.

In this study using our EC-SFA, we measured the current-distance profiles due to the electrochemical reaction of redox couples in an electrolyte confined between the Pt electrodes. We observed, for the first time, the sudden current increase of three orders of magnitude greater than the conventional feedback current at short distances on a nm level. We discussed the mechanisms of this sudden current increase at the short distance based on the measured double layer interactions. This study indicated that EC-SFA is useful for characterizing the electrochemical events under nano-confinement, which should be useful for the design of electrochemical systems such as sensors and energy devices.

2. Experiment

2.1. Materials

$\text{K}_3[\text{Fe}(\text{CN})_6]$ (99.5%, Nacalai Tesque), $\text{K}_4[\text{Fe}(\text{CN})_6]\cdot 3\text{H}_2\text{O}$ (99 %, Nacalai Tesque), and KClO_4 (99.99%, Aldrich) were used as received. The Pt plate (99.99%) from Toyoshima Manufacturing was used as a sputtering source. The Pt wire (99.9999, $\phi = 0.2$ mm) was purchased from Tanaka Kikinzoku. Ultrapure water (NANOpure II, Barnstead, 18 M Ω /cm resistance) was used after double distillation.

2.2. Preparation of Sample Surfaces

The Pt electrode surfaces were prepared by the mica-stripping method³⁶. A Pt film of ca.100 nm in thickness was deposited on freshly-cleaved mica by a sputtering deposition system (SPV-200, Toei Scientific Industrial) in an argon atmosphere as previously reported.³³ The as-deposited Pt films were glued on cylindrical quartz disks (curvature radius, $R = 20$ mm) by a hot-melt epoxy resin (E1004, Shell). For the EC-SFA measurements, a conductive wire was connected to the Pt surface using a conductive epoxy (CW2400, ITW Chemtronics), then covered by an epoxy resin. After removal of the mica template, a hydrophilic Pt surface was prepared.

2.3. Electrochemical Surface Forces Apparatus (EC-SFA)

A schematic illustration of the EC-SFA measurement system³¹ is shown in Fig 1 (a). Two prepared Pt electrodes were used as the working electrodes using a bipotentiostat (Model 2325, ALS) for controlling the electrochemical potential (E) and measuring the current (I). The counter electrode was a Pt-wire, and

the reference electrode was a Ag/AgCl (saturated KCl) electrode (BAS). The electrochemical measurements were performed inside the chamber of the twin-path SFA. The SFA chamber was filled with the aqueous electrolytes. Before all the measurements, argon (99.9999 %) was bubbled through the solutions for more than 30 min for deaeration, and the experiments were done under an argon atmosphere.

Force measurements were carried out by a twin-path SFA (RSM-1, Advance Riko) which determined the distance between the two surfaces by the modified two-laser beam interferometry technique.³¹ The interaction force (F) between the Pt electrode surfaces was measured as a function of the surface separation (D) in an aqueous solution. The spring constant of the cantilever was in the range of 160-220 N/m. We continuously changed the surface separation between the Pt surfaces at a constant approaching rate (20 nm/s) in order to obtain the force-distance profiles. The obtained force F was normalized by the radius R of the surface curvature using the Derjaguin approximation,¹⁸ $FR = 2\pi G_f$, where G_f is the interaction free energy per unit area between two flat surfaces. The observation of the electric double layer repulsion and hardwall contact (see results parts) confirmed the cleanliness of the electrode surfaces and the accuracy of the distance control with a nanometer resolution.

The measurement of the current-distance profiles was simultaneously performed along with the forces measurement. The potentials E of the upper and lower electrodes were $E = E_{\text{redox}} + \Delta V$ and $E =$

$E_{\text{redox}} - \Delta V$, respectively. We set $E_{\text{redox}} = 220$ mV, obtained from the cyclic voltammogram shown in Fig. S1 for the 0.1 mM aqueous solution of the $\text{Fe}(\text{CN})_6^{3-/4-}$ redox couple. We waited ca. 200 s before the current reached a constant value after setting the E values. The two electrodes were then approached from a distance greater than 2000 nm while measuring I and D by the bipotentiostat and twinpath interferometer, respectively, in order to obtain the current-distance profiles. The current-distance profiles of the anode and cathode of which the potentials were set at $E_{\text{redox}} + \Delta V$ and $E_{\text{redox}} - \Delta V$, respectively, showed the same absolute values of positive and negative currents as shown in Fig. S2, which supported the fact that the observed current should be due to the current between the two electrodes as illustrated in Fig. 1 (b). All measurements were done at room temperature (22 ± 2 °C).

3 Results and discussion

3.1 Forces between Pt surfaces in various electrolytes

Fig. 2 (a) shows a force-distance profile for the Pt electrode surfaces upon approach in the 0.1 mM aqueous solution of the $\text{Fe}(\text{CN})_6^{3-/4-}$ redox couple at $\Delta V = 0$ mV. The forces consisting of a long-range repulsion at $D < 30$ nm, which followed an exponential function, and the hardwall contact, were observed. The decay lengths of the repulsion were 6.5 ± 0.3 nm and in good agreement with the theoretical Debye

length ($1/\kappa$) for the current concentration of the electrolyte ($1/\kappa = 5.6$ nm), indicating that the observed repulsion was attributed to the electric double layer repulsion. It was reported that the potential of zero charge (pzc) of this electrode was ca. 0.2 V vs. Ag/AgCl.³³ Therefore, both the cathode and anode should be positively charged because the potentials of these electrodes were 0.22 V. The surface potentials (ψ_0) and charge density (σ) could be evaluated by fitting the profile to the Poisson-Boltzmann equation of the electric double layer force for the constant potential and charge model (See Figure S3), respectively^{18,37}. The evaluated ψ_0 and σ of the Pt electrode at $\Delta V = 0$ mV were 25.0 ± 2.2 mV and 0.30 ± 0.03 $\mu\text{C}/\text{cm}^2$, respectively, as summarized in Table 1.

At $\Delta V = 5$ and 50 mV, a similar long-range repulsion was observed, as shown in Fig. 2 (b) and (c), respectively. The decay lengths of the repulsion (6.3 ± 1.0 nm ($\Delta V = 5$ mV) and 5.7 ± 0.2 nm ($\Delta V = 50$ mV)) were similar to that at $\Delta V = 0$ mV and were in good agreement with $1/\kappa$ (5.6 nm), indicating that the observed repulsion was also attributed to the double layer repulsion. The appearance of the double layer repulsion showed that the sign of the two charged electrodes was the same perhaps due to ion adsorption even when the applied voltages were different in their sign. Assuming a symmetrical configuration, the σ values were obtained by fitting to the Poisson-Boltzmann equation to be 0.35 and 0.37 $\mu\text{C}/\text{cm}^2$ at $\Delta V = 5$ and 50 mV, respectively, as summarized in Table 1 together with the ψ_0 values. The

force-distance profiles upon separation under the same condition were also measured as shown in Fig S4.

No adhesion was observed at $\Delta V = 0$ mV and 5 mV, and a small adhesion force was observed at $\Delta V = 50$ mV.

We performed the same measurement for the Pt electrodes in the 1 mM aqueous $\text{Fe}(\text{CN})_6^{3-/4-}$ and 10 mM KClO_4 at various ΔV s. The electric double layer repulsion and the hardwall contact were observed in all cases (See supporting information). A small adhesion force was observed in the force profiles upon separation at $\Delta V = 5$ mV and 50 mV, while no adhesion was observed at $\Delta V = 0$ mV in the 1 mM $\text{Fe}(\text{CN})_6^{3-/4-}$. The σ values obtained by fitting to the Poisson-Boltzman equation are summarized in Table 1.

3.2 Currents between Pt surfaces in $\text{Fe}(\text{CN})_6^{3-/4-}$ solutions

We simultaneously performed current-distance measurements for the Pt electrodes with the forces measurement using the setup shown in Fig. 1 (b). Fig 3 (a) and (b) show a current-distance profile (an enlarged one in (b)) upon approach for the Pt electrodes in the 0.1 mM aqueous $\text{Fe}(\text{CN})_6^{3-/4-}$ redox couple at $\Delta V = 50$ mV. A gradual current increase of 10 nA (from 1.88 to 1.89 μA) was observed from $D = 2000$ nm to $D = 4.4$ nm. A sudden current increase from 1.89 μA to 12 mA was observed at $D = 4.4$ nm when D was further reduced as shown in Fig. 3 (b). This high current was constant from a separation of 4.4 nm

to the hardwall contact. When the electrodes were separated from the hardwall, the current was constant, ca. 12 mA, and suddenly decreased to 1.9 μA at $D = \text{ca. } 250 \text{ nm}$ and gradually decreased further to 1.81 μA at 20000 nm. The latter gradual current decrease was identical to that observed in the approaching process.

For understanding the detailed behavior of the sudden current increase at the short distance, the current-distance profiles for the Pt electrodes in the same solution at $\Delta V = 5$ and 0 mV were measured upon approach and separation as shown in Figs. 4 (a) and (b), respectively. At $\Delta V = 5$ mV, the sudden increase to 1 mA was observed at $D = 3.4 \text{ nm}$ when the electrodes were approached, as shown in Fig. 4 (a). This current was constant from $D = 3.4 \text{ nm}$ to the hardwall contact. When the surfaces were separated from the hard wall contact, the identical constant current was observed as the approaching process till $D = 3.3 \text{ nm}$, where a sudden current decrease was observed (Fig. 4 (b)). At $\Delta V = 0$ mV, we observed a similar sudden current increase and decrease at $D = 2.0 \text{ nm}$ during the approach and separation processes, respectively.³⁸ The amplitude of this current was 0.2 mA.

The effect of the $\text{Fe}(\text{CN})_6^{3-/4-}$ concentration was also studied. When the $\text{Fe}(\text{CN})_6^{3-/4-}$ concentration was increased to 1 mM, a gradual current increase of 400 nA from $D = 2000 \text{ nm}$ to 5 nm was observed at $\Delta V = 50 \text{ mV}$ during the approach, and this current was 40 times in magnitude greater than that for the 0.1

mM solution as shown in Fig. 5 (a). When the surfaces further approached, a sudden current increase to 0.4 mA was observed at $D=4.5$ nm (Fig. 5 (b)). This high current was constant until the hardwall contact. On the other hand, when the electrodes were separated from the hard wall contact at $\Delta V=50$ mV, the current was identical in magnitude as the approach process but the distance range was further extended to $D=100$ nm (Fig. 5 (c)) which was much longer than the 5 nm upon approach. At $\Delta V=5$ mV, the sudden increase to 0.4 mA was observed at $D=3.6$ nm when the electrodes were approached. This current was constant from $D=3.6$ nm to the hardwall contact. When the surfaces were separated from the hard wall contact, the current was identical in magnitude for the approach but the distance range was further extended to $D=50$ nm. At $\Delta V=0$ mV, we observed a slight sudden current increase and decrease (0.01 mA) at $D=ca. 2$ nm in the approach and separation processes, respectively.

We performed the same measurements in the 10 mM aqueous KClO_4 for studying the influence of the redox species on the current profile because this electrolyte showed no redox reaction over the entire range of E used in this study (0.17-0.27 V). There was no current change when the surfaces were approached at $D > 2.5$ nm as shown in Fig. 6 (a), which was different from the case of the $\text{Fe}(\text{CN})_6^{3-/4-}$ solutions (Fig. 4 and 5). A sudden current increase to 3.8 mA at $D=2.5$ nm was observed upon the approach when $\Delta V=50$ mV (Fig 6 (b)). The same sudden current increases were observed in the case

of $\Delta V = 0$ and 5 mV at $D = 2.5$ and 2.3 nm, respectively, which were practically identical as that at $\Delta V = 50$ mV. The same current profiles were observed during the separating process as those during the approaching process for all three ΔV cases, as shown in Fig. 6 (b). On the other hand, the D values increased with the increasing ΔV in the case of the 0.1 mM $\text{Fe}(\text{CN})_6^{3-/4-}$ solution (2.0, 3.4 and 4.4 nm at 0, 5, and 50 mV, respectively). The obtained results from the 10 mM aqueous KClO_4 (shorter D_C than that of the $\text{Fe}(\text{CN})_6^{3-/4-}$ solution, no dependence of D_C on ΔV and no hysteresis between approaching and separating processes) were different from those in the case of the $\text{Fe}(\text{CN})_6^{3-/4-}$ solution.

3.3 Discussion

As described in section 3.2, the gradual current increase at the longer D and sudden increase at the shorter D were observed in the current profiles for the Pt electrodes in the $\text{Fe}(\text{CN})_6^{3-/4-}$ solutions. In this section, the origin of these two current increases is discussed.

First, we discuss the origin of the gradual current increase at the longer D . The amplitude of the current change in the 1 mM $\text{Fe}(\text{CN})_6^{3-/4-}$ solution was 40 times in magnitude greater than that for the 0.1 mM $\text{Fe}(\text{CN})_6^{3-/4-}$ solution as shown in Fig. 3 (a) and Fig. 5 (a). Such a distance dependent increase was not observed in the case of the 10 mM KClO_4 solution as shown in Fig. 6 (a). These results indicated that

the current change in the $\text{Fe}(\text{CN})_6^{3-/4-}$ solutions can be attributed to the feedback current due to the redox cycle reaction which resulted in the gradual current amplification observed when the cathode and anode were brought closer at a μm level distance in the redox couple solution.⁹ On the other hand, the sudden current increase occurred at a nm distance, and its amplification reached 10^6 times. This phenomenon can be at least different in origin from the already known feedback current.

Second, we discuss the origin of the behavior in the short distance range. In order to analyze the behavior more in detail, the amplitude of the sudden current change (I_c) and the critical distance (D_c) are plotted vs. ΔV in Fig. 7 (a) and (b), respectively. I_c linearly increased when the ΔV was increased in both of the 0.1 and 1 mM $\text{Fe}(\text{CN})_6^{3-/4-}$ solutions as shown in Fig. 7 (a). The I_c values of the 0.1 mM solution were 3 times higher than those of the 1 mM $\text{Fe}(\text{CN})_6^{3-/4-}$ solution, which was the opposite trend of the conventional feedback current observed in the long D range. Concerning D_c , the current hysteresis was observed between the approach and the separation processes in both of the 0.1 and 1 mM $\text{Fe}(\text{CN})_6^{3-/4-}$ solutions except for those at $\Delta V = 5$ mV in the 0.1 mM solution which exhibited the same D_c values in both the approach and separation processes (Fig. 7 (b)-(c)). Such a current hysteresis was not found at 0 mV, which showed only a minor current increase (Fig. 5 (c)). For the KClO_4 solution, there was no current hysteresis as shown in Figs. 6 (b) and (c).

A possible mechanism of the sudden current change at the short D is proposed based on the simultaneously measured force profiles. The double layer repulsion forces observed at D_c in the 0.1 mM $\text{Fe}(\text{CN})_6^{3-/4}$ solution at 0, 0.5, and 50 mV were 0.49 ± 0.08 mN/m, 0.51 ± 0.08 mN/m and 0.49 ± 0.03 mN/m, respectively (see Fig. 2 (a)-(c)). It is interesting that the double layer repulsion observed at D_c was nearly identical for all the cases. The double layer repulsion was produced by the osmotic pressure of the counterions in the electric double layer, thus the amplitude of the repulsion was determined by the concentration of the total confined electrolyte species. The sudden current increase could be correlated with the identical double layer repulsion at D_c , which could provide the threshold concentration of the redox species in the double layer. Therefore, we tried to evaluate the threshold concentration of the redox species at D_c using a previously reported model for calculating the confined ion concentration in the electric double layer.⁴ This model can calculate the ion concentration between two electrodes (Figure S8) by integrating the ion distribution in the double layer estimated from the ψ_0 and $1/\kappa$ values obtained using the measured force profiles. The calculated concentration was 8.3 ± 0.3 mM (80 times more concentrated than the bulk value) for the 0.1 mM aqueous $\text{Fe}(\text{CN})_6^{3-/4}$ at 50 mV. The average distance between the redox molecules at this concentration was 2.2 nm (9.7 nm in the bulk solution). The threshold concentration for the 1 mM aqueous $\text{Fe}(\text{CN})_6^{3-/4}$ at 50 mV was calculated to be 18.5 ± 5.4 mM (18 times

more concentrated than the bulk values). This value was similar to that for the 0.1 mM solution because the error at this concentration was high due to the short Debye length of 1.7 nm.

We may discuss how the redox reactions proceeded in such concentrated solutions of redox species confined in the nanospace, which resulted in the sudden current increase at D_c . Such a long distance of the electron transfer current between the electrodes suggested that the molecular organization of $\text{Fe}(\text{CN})_6^{3-/4-}$ formed under confinement, which enhanced the collisions and/or electron transfer (or hopping) between the redox species. The current hysteresis, longer D_c upon separation, accompanied observation of adhesion force at $\Delta V = 50$ mV in the 0.1 mM $\text{Fe}(\text{CN})_6^{3-/4-}$ solution and at $\Delta V = 5$ and 10 mV in the 1 mM $\text{Fe}(\text{CN})_6^{3-/4-}$ solution. This supported the presence of assembled redox species under confinement.

4. Conclusion

We studied the electrochemical current between electrodes under nano-confinement in the presence of redox species using our EC-SFA. Our results are summarized as follows:

(1) Based on the current-distance profiles for two Pt electrodes in aqueous $\text{Fe}(\text{CN})_6^{3-/4-}$, the gradual current increases at a long distance and the sudden current increase at a short distance (~ 5 nm on approach and ~ 200 nm on separation) were observed, the latter for the first time.

(2) The amplitude of the gradual current increases (~ 400 nA with 2000 nm D changes) at a long distance increased with the increasing $\text{Fe}(\text{CN})_6^{3-/4-}$ concentration. In contrast, we did not find this current change in the case of the aqueous KClO_4 . These results indicated that the current increase in the greater distance range was due to the conventional feedback current of the redox cycling.

(3) The amplitude of the sudden current increase at short distances decreased with the increasing $\text{Fe}(\text{CN})_6^{3-/4-}$ concentration. The current suddenly increased at D_c which was longer for the greater ΔV . In addition, we found greater D_c values upon separation than those on approach when ΔV was high ($\Delta V = 50$ mV for 0.1 mM solution and $\Delta V = 5$ mV \sim for 1 mM solution). In the case of the aqueous KClO_4 , the distance range of the sudden current change, D_c , was smaller than that of the $\text{Fe}(\text{CN})_6^{3-/4-}$ solution with no dependence on ΔV . There was also no current hysteresis between the approaching and separating processes in the aqueous KClO_4 . These results indicated that the presence of redox species strongly affect this sudden current change.

(4) The force profiles simultaneously obtained with the current-distance profiles showed that the same amplitude of the double layer repulsion was observed at D_c for all three ΔV values on approach, suggesting that the concentrated and/or assembled redox species induced the sudden current increase due to chain

reaction of electron transfer between the redox species. There was a threshold concentration of the redox species for this phenomenon.

These results revealed the insight into the electrochemical reactions under the nano-confinement. We believe that the EC-twin-path SFA we developed will become a powerful tool for obtaining fundamental knowledge about the nano-confined electrochemical reactions for nanoelectrodes which can be applied to sensors and energy devices.

Conflicts of interest

There are no conflicts to declare.

Acknowledgment

This work was supported by the CREST program of the Japan Science and Technology Agency (JST), the Regional Innovation Ecosystem Program (MEXT), and JSPS KAKENHI Grant Numbers / 26248002.

References

- 1 C. Aliaga, C. S. Santos and S. Baldeli, *Phys. Chem. Chem. Phys.*, 2007, **9**, 3683-3700.
- 2 K. Ueno, M. Kasuya, M. Watanabe, M. Mizukami and K. Kurihara, *Phys. Chem. Chem. Phys.* 2010, **12**, 4066-4071.
- 3 S. Ito, A. Unemoto, H. Ogawa, T. Tomai and I. Honma, *J. Power Sources*, 2012, **208**, 271-275.
- 4 M. Kasuya, Y. Sano, M. Kawashima and K. Kurihara, *Langmuir* 2021, **37**, 5073–5080.
- 5 D. W. M. Arrigan, *Analyst*, **129**, 1157-1165.
- 6 S. Pennathur, J. C. T. Eijkel and A. van der Berg, *Lab Chip* 2007, **7**, 1234-1237.
- 7 F.-R. F. Fan, A. J. Bard, *Science* **1995**, 267, 871–874.
- 8 C. Mao, N. M. Contento, L. R. Gibson and P. W. Bohn, *ACS Nano*, 2013, **7**, 5483-5490.
- 9 A. J. Bard, J. A. Crayston, G. P. Kittlesen, T. V. Shea and M. S. Wrighton, *Anal. Chem.*, 1986, **58**, 2321–2331.
- 10 K. Ueno, M. Hayashida, J. Y. Ye and Misawa H., *Electrochem. Commun.*, 2005, **7**, 161-165.
- 11 P. S. Singh, H. S. M. Chan, S. Kang and S. G. Lemay, *J. Am. Chem. Soc.*, 2011, **133**, 18289-18295.
- 12 S. Pennathur and J. G. Santiago, *Anal. Chem.*, 2005, **77**, 6782-6789.
- 13 A. Eden, K. Scida, N. Arroyo-Curras, J. C. T. Eijkel, C. D. Meinhart and S. Pennathur, *Electrochimica Acta*, 2020, **330**, 135275.
- 14 A. Schulte and W. Schumann, *Angew. Chem.*, 2007, **119**, 8760-8777.
- 15 Y. Takahashi, A. I. Shevchuk, P. Novak, Y. Murakami, Y. Zhang, N. Ebejer, J. V. Mapherson, P. R. Unwin, A. J. Pollard, D. Roy, C. A. Clifford, H. Shiku, Matsue T. D. Klenerman and Y. E. Korchev, *Angew. Chem. Int. Ed.*, 2011, **50**, 9638-9642.

- 16J. V. Macpherson, P. R. Unwin, A. C. Hillier, and A. J. Bard, *J. Am. Chem. Soc.* 1996, **118**, 6445–6452.
- 17A. Anne, E. Cambriil, A. Chovin, C. Bemille and C. Goyer, *ACS Nano*, 2009, **3**, 2927-2940.
- 18J. N. Israelachvili, *Intermolecular and Surface Forces, 3rd ed.*; Academic Press, Ltd.: New York, **2010**.
- 19R. G. Horn and J. N. Israelachvili, *J. Chem. Phys.* 1981, **75**, 1400–1411.
- 20J. N. Israelachvili, P. M. McGuiggan and A. M. Homola, *Science* 1988, **240**, 189-191.
- 21J. V. Alsten and S. Granick, *Phys. Rev. Lett.* 1988, **61**, 2570-2573.
- 22J. Klein and E. Kumacheva, *Science* 1995, **269**, 816-818.
- 23C. D. Dushkin and K. Kurihara, *Colloids Surfaces A: Physicochem. Eng.* 1997, **129-130**, 131-139.
- 24M. Mizukami and K. Kurihara, *Rev. Sci. Instrum.* 2008, **79**, 113705.
- 25H. Sakuma, K. Otsuki and K. Kurihara, *Phys. Rev. Lett.* 2006, **96**, 046104.
- 26S. Nakano, M. Mizukami, N. Ohta, N. Yagi, I. Hatta and K. Kurihara *Jpn. J. Appl. Phys.* 2013, **52**, 035002.
- 27D. Fukushi, M. Kasuya, H. Sakuma and K. Kurihara, *Chem. Lett.* **2011**, **40**, 776-778.
- 28T. Kamijo, M. Kasuya, M. Mizukami and K. Kurihara, *Chem. Lett.* 2011, **40**, 674–675.
- 29J. Fréchette and T. K. Vanderlick, *Langmuir* 2001, **17**, 7620–7627.
- 30J. N. Connor and R. G., Horn, *Langmuir* 2001, **17**, 7194–7197.
- 31H. Kawai, H. Sakuma, M. Mizukami, T. Abe, Y. Fukao, H. Tajima and K. Kurihara, *Rev. Sci. Instrum.* 2008, **79**, 043701.
- 32M. Kasuya, T. Sogawa, T. Masuda, T. Kamijo, K. Uosaki and K. Kurihara, *J. Phys. Chem. C* 2016, **120**, 15986–15992.

33 S. Fujii, M. Kasuya and K. Kurihara, *J. Phys. Chem. C* 2017, **121**, 26406–26413.

34 M. Kasuya and K. Kurihara, *Langmuir* 2014, **30**, 7093–7097.

35 F.-R. F. Fan and A. J. Bard, *J. Am. Chem. Soc.* 1987, **109**, 6262–6268.

36 M. Hegner, P. Wagner and G. Semenza, *Surf. Sci.* 1993, **291**, 39–46.

37 D. Y. C. Chan, R. M. Pashley and L. R. A White, *J. Colloid Interface Sci.* 1980, **77**, 283–285.

38 One may think why the current was observed even $\Delta V = 0$ mV. We supposed that it may be due to tiny difference of the electrode potential (< 1 mV) between two electrodes.

Table 1 Surface potential, ψ_0 , and charge density σ of Pt electrodes in aqueous solution of $\text{Fe}(\text{CN})_6^{3-/4-}$ redox couple obtained from fitting the force-distance profiles by the Poisson–Boltzmann equation.

Concentration	ΔV [mV]	ψ_0 [mV]	σ [$\mu\text{C}/\text{cm}^2$]	decay length [nm]	$1/\kappa$ [nm]
0.1 mM	0	25.0 ± 2.2	0.30 ± 0.02	6.2 ± 0.9	5.6
0.1 mM	5	28.3 ± 3.0	0.35 ± 0.03	6.2 ± 0.9	5.6
0.1 mM	50	33.3 ± 2.9	0.37 ± 0.03	6.2 ± 0.9	5.6
1.0 mM	0	6.6 ± 1.5	0.35 ± 0.15	2.5 ± 0.2	1.7
1.0 mM	5	8.5 ± 2.2	0.48 ± 0.13	2.2 ± 0.3	1.7
1.0 mM	50	9.8 ± 2.0	0.53 ± 0.10	2.3 ± 0.8	1.7

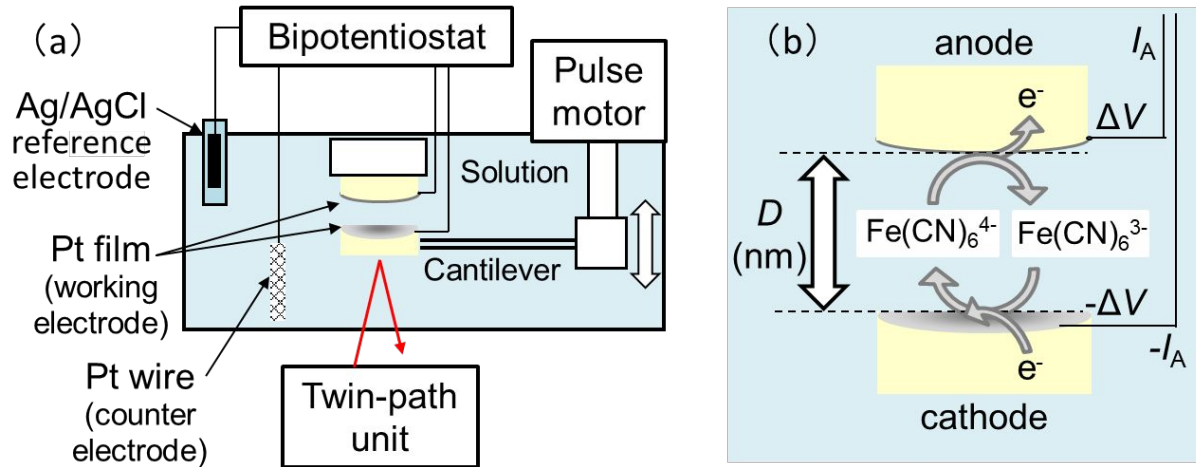


Fig.1 (a) Schematic illustration of EC-SFA. (b) Schematic illustration of nano-confined electrochemical reaction between the electrodes surfaces.

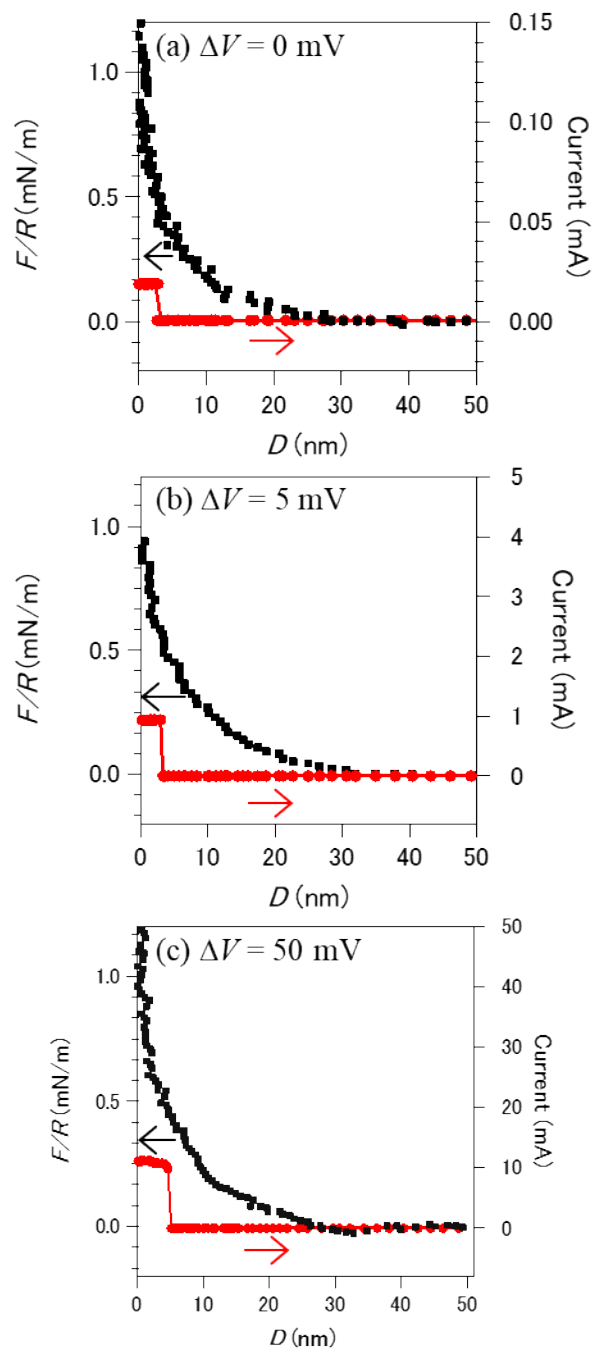


Fig. 2 Profiles of forces between Pt electrode surfaces in 0.1 mM aqueous solution of $\text{Fe}(\text{CN})_6^{3-/4-}$ redox couple depending on the applied potentials: (a) 0 mV, (b) 10 mV, (c) 50 mV. Current profiles (red circles) simultaneously measured were also plotted in the same Figure.

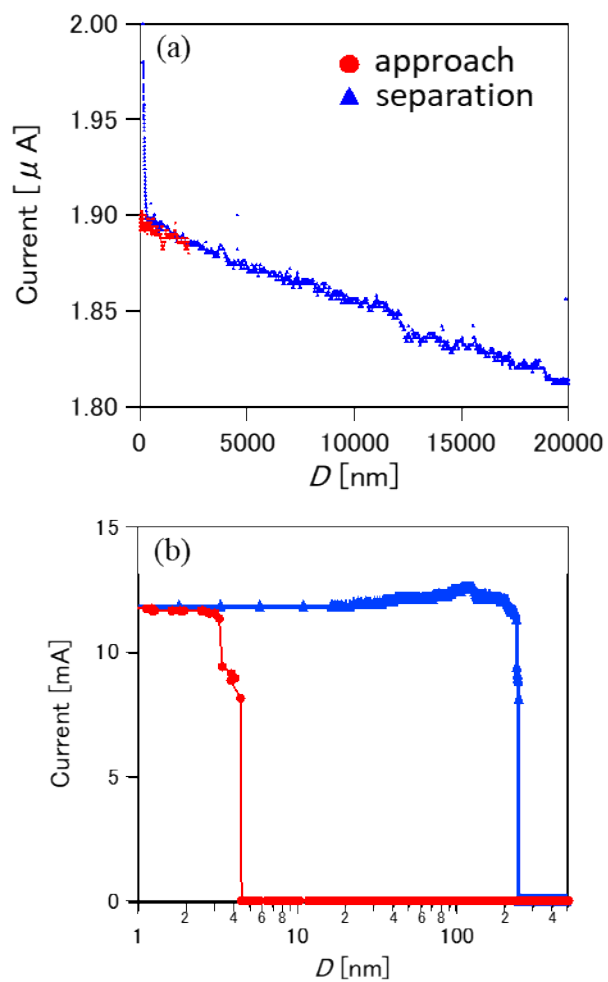


Fig. 3 Current profiles for the Pt electrode surfaces in 0.1 mM $\text{Fe}(\text{CN})_6^{3-/4-}$ solution during approach (red circles) and separation (blue triangles) in μm range (a) and nm range (b). $\Delta V=50$ mV.

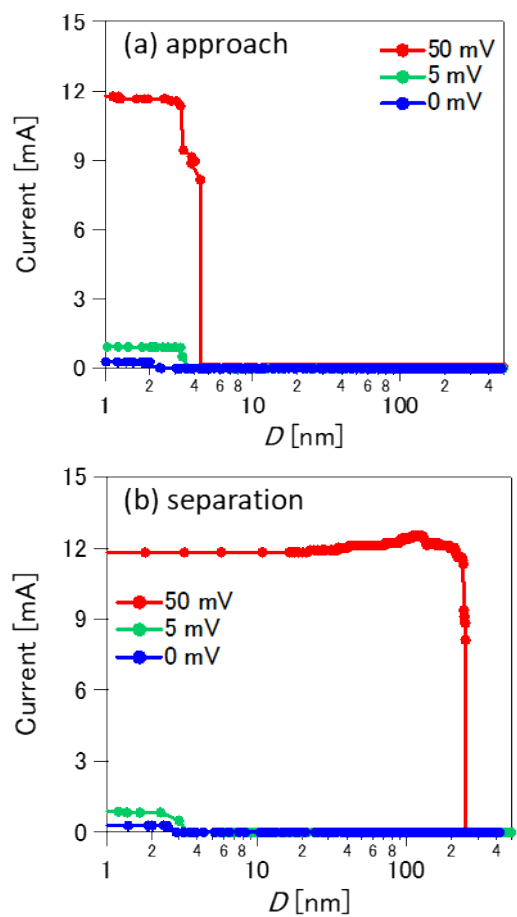


Fig. 4 Current profiles for the Pt electrode surfaces in 0.1 mM aqueous $\text{Fe}(\text{CN})_6^{3-/4-}$ at various ΔV values during approach (a) and separation (b) in nm range.

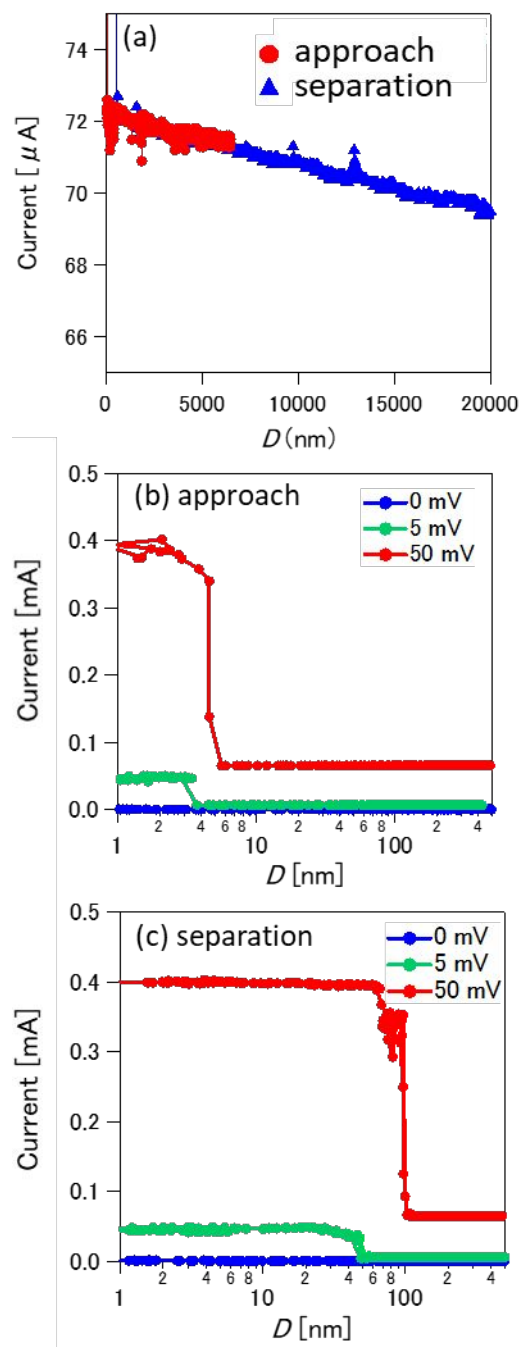


Fig. 5 (a) Current profiles for the Pt electrode surfaces in 1 mM $\text{Fe}(\text{CN})_6^{3-/4-}$ solution during approach (red circles) and separation (blue triangles) in μm range ($\Delta V = 50 \text{ mV}$). Same current profiles at various ΔV values in nm range during approach (b) and separation (c) are shown.

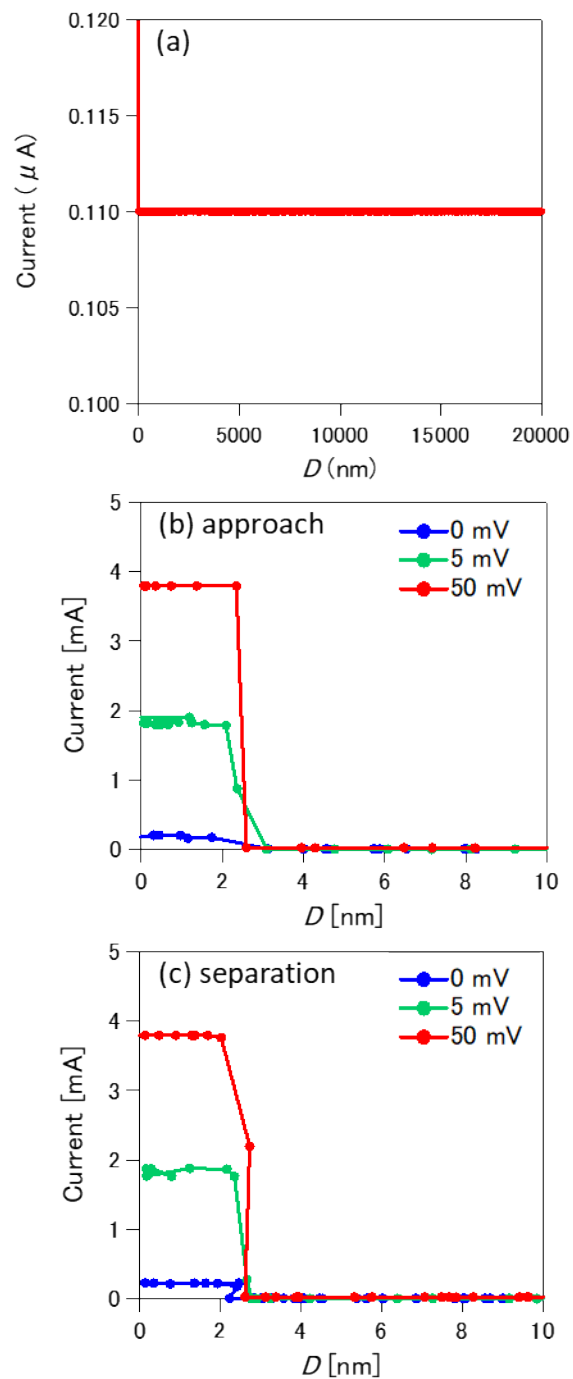


Fig. 6 (a) Current profiles for the Pt electrode surfaces in 10 mM KClO₄ solution during approach in μm range ($\Delta V=50$ mV). Same current profiles at various ΔV values in nm range during approach (b) and separation (c) are shown.

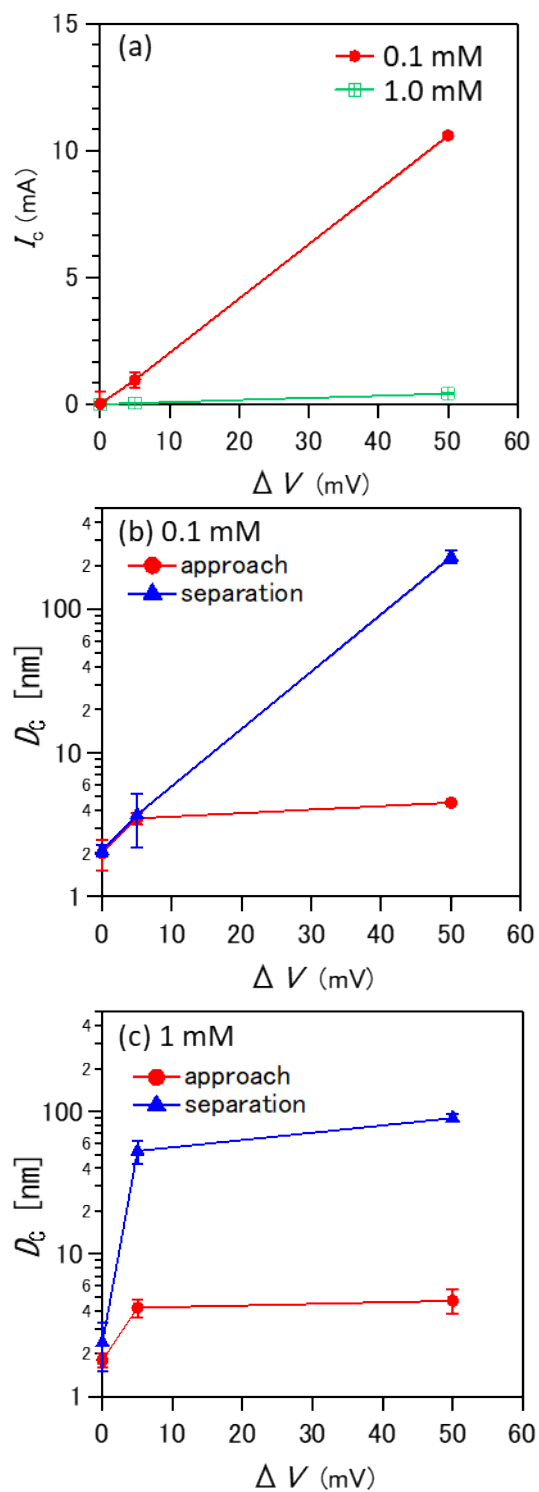


Fig. 7 Amplitude, I_A , (a) and distance range, D_c , (b) and (c) of the sudden current increases at the short distance depending on ΔV , obtained from the current-distance profiles in aqueous $\text{Fe}(\text{CN})_6^{3-/4-}$.

